nature materials

SUPPLEMENTARY INFORMATION

DOI: 10.1038/NMAT4407

Matrix elasticity of void-forming hydrogels controls transplanted-stem-cell-mediated bone formation

Nathaniel Huebsch, Evi Lippens, Kangwon Lee, Manav Mehta, Sandeep T Koshy, Max C Darnell, Rajiv Desai, Christopher M. Madl, Maria Xu, Xuanhe Zhao, Ovijit Chaudhuri, Catia Verbeke, Woo Seob Kim, Karen Alim, Akiko Mammoto, Donald E. Ingber, Georg N Duda, and David J. Mooney

Supplemental Materials

Methods

Fabrication of Void-Forming Hydrogels

Hydrogel porogens Sodium alginate with high molecular weight and high guluronic acid (GA) content (MVG) was purchased from FMC Biopolymer (Princeton, NJ). Pharmaceutical grade material was used for materials characterization and *in vitro* studies, while ultrapure, medical grade material was used for *in vivo* studies. To facilitate polymer hydrolysis, alginates were oxidized with sodium periodate (Sigma) to form alginate dialdehyde with a theoretical degree of between 3-7.5% of GA residues converted to aldehyde groups[1,2]. Oxidation reactions were quenched with ethylene glycol (Sigma), and polymers were dialyzed against water using 3.5 kDa cutoff membranes. After dialysis, polymers were decoloured with activated charcoal, sterile filtered (0.2μm) and lyophilized. In some experiments, alginate dialdehyde polymers were further labeled with aminofluorescein (Invitrogen) using the protocol developed by Kong *et al*[3].The molar ratios between aminofluorescein and uronic acids of alginate was adjusted so that 2 aminofluorescein molecules on average were coupled to each polymer chain. In certain experiments, high molecular weight MVG was labeled with Tetramethylrhodamine 5-(and-6)-carboxamide cadaverine (TAMRA cadaverine; Anaspec, Fremont, CA). On average, 8 TAMRA cadaverine molecules were coupled to each polymer chain. Freeze-dried polymer formulations were reconstituted to 20-50 mg/mL in serum free Dulbecco's Modified Eagle Medium (DMEM; Invitrogen). To enhance the mechanical integrity of porogens during processing steps and encapsulation, alginate dialdehyde was mixed with various amounts of unlabeled high M_w MVG, which was dialyzed and decoloured in a similar manner. The different alginate formulations used to form porogens are listed explicity in Table S.1.

Initially, the influence of alginate composition on initial mechanical properties and subsequent degradation of the polymers that were used to fabricate porogens were tested using hydrogel discs, which were formed by mixing alginate polymers with a constant amount (4% v) of calcium-sulfate slurry (1.22 M). After gel formation, mechanical properties were tested on an Instron 3342 Mechanical Apparatus (Instron; Norwick, MA) under unconfined compression (1mm/minute). The elastic modulus *E* was

DOI: 10.1038/NMAT4407

calculated as the slope (first 10% of strain) of the stress vs. stain curves (fig. S1). Hydrogel degradation in DMEM was assessed by monitoring the dry mass over time of hydrogels. Sodium Azide (0.1% wt) was added as a preservative in degradation studies.

For all subsequent studies using porogens, a calcium-chloride bath was used for crosslinking of porogen. To form hydrogel bead porogens, mixtures of MVG and alginate dialdehyde were suspended to 2-8% wt in serum free DMEM and extruded via syringe pump (Harvard Apparatus; Holliston, MA) through a glass atomizer with co-axial nitrogen air flow at a constant pressure of 20-40 mmHg (measured using a Flowmeter; Scott Specialty Gases, Plumsteadville PA). Alginates were extruded into a bath of calcium chloride (25-100mM, Sigma) in 100mM HEPES buffer (pH 7.4; Sigma) with constant stirring. After 5 minutes of crosslinking in the $CaCl_2$ bath, microspheres were retrieved, centrifuged (3100 rpm for 10 minutes), then washed twice in DMEM. In some experiments, the size distribution of aminofluorescen-labeled porogens was assessed. The gross appearance of porogens was assessed with fluorescent micrographs obtained on an Olympus IX81 inverted microscope. Quantitative analysis of porogen diameter was performed using the Matlab Image Processing Toolbox (Mathworks; Natick, MA) on n = 100 randomly selected porogens.

"Bulk" Hydrogel Synthetic ECM Analogs To form the cell-interactive bulk hydrogel phase, sodium alginate with high molecular weight and high guluronic acid content (MVG) was obtained from FMC biopolymer. In some cases, MVG was combined with low M_w MVG, which was obtained by irradiating MVG with a 5 Mrad Cobalt source to produce a low molecular weight alginate with high GA content. When this low M_w material is mixed with a critical amount of high M_w MVG, the binary mixture (binary MVG) crosslinks to a high degree in the presence of divalent cations, but has a pre-hydrogel viscosity similar to that of pure MVG at low concentrations[4]. The lower viscosity of binary MVG pre-polymer solution (compared to pre-polymer solution formed by the same weight percent of unary MVG) facilitates cell encapsulation without loss of cell viability[5]. The weight-averaged molecular weight M_w and gyration radius r_g were previously calculated using gel permeation chromatography[5].

Following aforementioned chain modifications, the adhesion peptide sequence G_4RGDASSP-OH was coupled to MVG. All peptides were purchased from Peptides International (Louisville, KY) and characterized at > 95% purity by the manufacturer. Peptides were coupled to alginate polymers using published carbodiimide chemistry[6]. Following peptide modification, alginate was dialyzed and decoloured as described above. Lyophilized MVG was reconstituted to 4% wt in media without serum or phenol red.

To form standard, nanoporous alginate hydrogels, a calcium sulfate slurry (1.22M in deionized water; Sigma) was mixed with 1-2% wt solutions of MVG and crosslinked using luer-lock syringes. The final concentrations of MVG and calcium sulfate, the crosslinking agent, used to obtain gels of specific elastic moduli[2] are given in Table S.2. Except in studies where the elastic modulus of the bulk component was varied, the bulk component of void-forming hydrogels, as well as the single-phase of standard hydrogels, was formulated to yield an initial elastic modulus of 60 kPa. Hydrogels were cast between glass plates separated by a spacer (1-5mm). Alginate hydrogels were crosslinked for 45 minutes before discs were punched out and transferred to media.

Composite void-forming gel formation Alginate porogens prepared as described above were mixed into a solution of 1-2% wt/wt MVG with 0-4% additional high M_w MVG using luer lock-syringes. These solutions were then mixed with calcium sulfate slurry to a final concentration of 6.25-50mM Ca^{2+} in the bulk alginate polymer phase to form multi-phase hydrogels (1-5mm thickness).

Fluorescence Assay for Characterization of Void-Formation Micron-scale pore formation within multi-component matrices was first monitored qualitatively by obtaining scanning electron micrographs (SEM) of materials that were flash-frozen in liquid nitrogen and then freeze-dried. SEM were obtained at the Harvard University Center for Nanoscale Systems (fig. S2). Previous work has demonstrated that flash-freezing hydrogels introduces only a very small degree of pore formation[8], such that this preparation step would be expected to have a minimal effect on existing pores.

To verify void formation, while avoiding any potential freezing-induced artifacts, a fluorescence assay was developed. In this assay, aminofluorescein-labeled porogens were encapsulated into bulk gel comprised of TAMRA cadaverine modified MVG. The distribution of aminofluorescein-modified porogen beads within non-degradable gel matrices was assessed by obtaining representative micrographs of the beads within transparent bulk hydrogels, or bulk hydrogels consisting of rhodamine-labeled alginate immediately after hydrogel formation (fig. S1, 1b). Void-formation was confirmed via disappearance of the fluorescein signal without substantial reduction in the TAMRA signal, as assessed by confocal microscopy on days 0, 1, 7 and 14 after gel formation (fig. 1b).

To quantify the kinetics of porogen degradation and subsequent void formation, we performed quantitative fluorescence analysis, in which the fluorescence of aminofluorescein remaining in hydrogels was used a surrogate metric for the amount of intact porogen remaining. The accumulation of aminofluorescein in the media was also used as a metric of porogen degradation, as well as to verify that the total amount of aminofluorescein (within porogens inside of gels, and within media) remained constant. To avoid spectral cross-talk between aminofluorescein and TAMRA cadaverine in these studies, we used gels in which only the porogen component was fluorescently labeled. At each time-point, the media bathing gels was carefully aspirated, without mechanically perturbing the gel, and the gel was then washed with PBS. Next, the composite void-forming hydrogels were dissolved completely (50mM EDTA in PBS). The amount of aminofluorescein present in gels and accumulated in media was then measured using a SpectraMax plate reader with excitation at 490nm and emission at 520nm. Linearity of the relationship between fluorescein concentration and fluorescence signal was confirmed with serial dilutions of the PBS/EDTA or media solutions. The data shown in Figure 1 are representative of what we observed in three independent experiments.

Mechanical Characterization of Void-Formation Alginate hydrogels (12.2mm diameter and 2mm thickness) with or without porogens were equilibrated into serum free DMEM for 2 hr and then subjected to a strain sweep using a rheometer (Bohlin). During the strain sweep frequency sweep (0.01 to 3% strain), samples were maintained at a 1% compressive strain, and tested at a frequency of 1 Hz. Rheologic analyses (fig. 1) were

DOI: 10.1038/NMAT4407

further verified with unconfined compression testing (1mm/minute) using an Instron 3342 mechanical apparatus as described above. The fracture toughness of the gels was also measured, following the standard pure-shear test[7]. For pore-formation analysis via measurements of the time-course of shear modulusequilibrated hydrogels were transferred to serum free DMEM with 0.1% sodium azide, and media was changed daily for 1-7 days.

Mesenchymal Stem Cell Deployment and Fate Studies

Interconnected Void Formation and Minimum Porogen Density Requirements for Cell Release The formation of interconnected pores was monitored with a capillary assay. Briefly, scaffolds were maintained in DMEM with sodium azide and at each of several time-points, the wet weight of scaffolds (w_{wet}) was obtained. Immediately after this, filter paper was held onto the surface of the hydrogel, and water within micro-scale and larger pores was withdrawn via capillary action. The weight of the wicked hydrogel w_{wicked} was next obtained. The relative void volume was calculated according to Equation 1:

$$V = \frac{w_{wet} - w_{wick}}{w_{wet}} \qquad \text{Equation 1}$$

where V is the fraction of total weight occupied by interconnected voids. Note this calculation assumes the weight of water within the nanometer-scale pores of the hydrogel comprises most of the weight of the material.

As encapsulated porogens are randomly distributed throughout bulk hydrogels, it was expected that a porogen volume fraction of at least 65% - the threshold for percolation (supplemental ref. 9) – would be required for efficient cell release. The kinetics of interconnected void formation throughout void-forming hydrogels were analyzed with a capillary assay, which indicated that voids continued forming over a period of 7-12 days after gel formation, and also confirmed a requirement for a porogen density exceeding the percolation threshold of 65% to efficiently form interconnected pores (fig. S3). However, as composite void-forming materials became less fracture resistant over time with increased porogen volume fractions, (fig. S2), systematic analysis was done to identify the minimum porogen volume fraction that would allow efficient cell deployment.

Although the formation of interconnected void-networks across an infinitely large medium would require a 65% porogen fraction p_c, numerical predictions regarding the formation of interconnected networks of voids throughout finitely-sized media predict a substantial number of "lattice-spanning void clusters" when the ratio of the porogen diameter d to the overall gel dimension D increases[10]. Consider P_n, the probability of finding a connected "cluster" of voids that contains n voids. P_n is defined via the number N_n, of clusters each containing n voids:

$$P_n(p) = \frac{N_n(p)}{\sum_n N_n(p)} \qquad \text{Equation 2}$$

In general, the number of clusters of a certain size is known only to follow a scaling relation for large values of p, near the percolation threshold. For sub-percolation values of p, as in the scenario tested here, the number N_n is exactly enumerated by the following formula:

$$N_n(p) = \sum_{configurations} M_{n,j} \times p^n \times (1-p)^m \qquad \text{Equation 3}$$

Here, the number of clusters of n voids is the sum over all different possible spatial configurations, with the number of each individual configuration being proportional to the number of mutually equivalent configurations $M_{n,j}$ (e.g. rotations in space of a group of n voids) times the probability of having n voids in the first place (p^n) times the probability of *not* having pores surrounding a 'perimeter' within length j of the void cluster $(1-p)^j$.

We proposed to abstract the above formula by assuming a *general* perimeter of three dimensional clusters, $j = 4n$. Then the value N_n can be approximated as:

$$N_n(p) = M_n \times p^n \times (1-p)^m \qquad \text{Equation 4}$$

To estimate the connectivity of sub-percolation density particles in a lattice of arbitrary dimension, Care and Ettelaie have provided numerical estimates of the value M_n (supplemental ref. 10), and these values were used here.

Given the probability of finding connected clusters of n porogens for many values of n, we next estimate the overall number of cells egressing a porous gel via pores in the gel, by assuming that this number is proportional to the surface area A of all pore clusters connected to the surface of the gel. Given P_n, and a composite gel of volume V and surface area S, laden with spherical porogens of surface area σ and radius $d/2$ and a porogen volume density of p, a crude estimate of the area accessible from the gel's surface is given by the product of the probability to find a pore connected to the surface times the average area of a pore cluster (Equation 5).

$$A = \frac{pSd}{V} \times \sum_n \sigma n P_n(p) \qquad \text{Equation 5}$$

Finally, to provide a normalized estimate for the probability of cell release, we assumed that any encapsulated cell within a distance γ of these "surface-connected voids" would be capable of egressing from the hydrogel. Therefore, the approximate probability that a cell could be deployed from the material was given by

$$P(deploy) = \frac{\gamma A}{V} \qquad \text{Equation 6}$$

γ was set to 10μm, or the approximate diameter of MSC. Because the cells were encapsulated into cylindrical hydrogels, wherein the cylinder radius is much larger than its height (typical gel dimensions were 12.2mm diameter at 2mm height), the quantities S and V were calculated for a cube of arbitrary volume at the center of the cylinder (fig. S3). The height of the cube was fixed at Nd, or an arbitrary number N times d, the

DOI: 10.1038/NMAT4407

diameter of one porogen (for these estimates, $d = 200\mu m$). Based on these parameters, the approximate value for $P(\text{deploy})$ was calculated numerically as

$$P(deploy) \approx \frac{6\gamma p}{N^4 d} \sum n \times P(n) \qquad \text{Equation 7}$$

These numerical predictions were consistent with data obtained on the net deployment of mMSC from void forming hydrogels over 14 days (fig. S3). In particular, the curves predicted for $P(\text{deploy})$ for values of p less than the percolation threshold of 0.65 predicted the relationship between the actual values $P(\text{deploy})$ that were measured in cell release assays as the value Nd increased. Based on these results, all subsequent studies of cell deployment were performed with a 50% porogen volume fraction, to maximize cell release while maintaining the structural integrity of the composite scaffold.

Routine Cell Culture Human mesenchymal stem cells (hMSC; supplemental ref. 11) were purchased from Lonza (Basel, Switzerland). hMSC were maintained in low glucose DMEM supplemented with 20% FBS and 1% penicillin/streptomycin (Invitrogen), and used between passages 2-6. Clonally derived murine bone marrow stromal mesenchymal stem cells (mMSC), originally obtained from Balb/c mice (D1; supplemental ref. 12) were purchased from American Type Cell Culture (ATCC) and maintained in standard DMEM supplemented with 10% Fetal Bovine Serum and 1% penicillin/streptomycin (Invitrogen), and used between passages 20-24. Cells were maintained at lower than 80% confluency in culture.

In vitro proliferation studies To assess S-phase progression, mMSC that had been grown either within standard or void-forming hydrogels were exposed to ^{3}H-labeled thymidine (2μCi; Perkin Elmer) over 24 hr. Gels were then carefully washed to remove unincorporated ^{3}H-thymidine, and chelated (50mM EDTA). Cell pellets were lysed into 12 M NaCl, and ^{3}H-thymidine incorporation was analyzed using a scintillation counter (Amersham Pharmacia).

Cell proliferation was also assessed by Ki-67 staining. Briefly, void-forming hydrogels were fixed (4% paraformaldehyde to crosslink cells, followed by 100mM barium chloride to crosslink hydrogels), washed extensively in PBS, embedded into OCT and flash frozen in liquid N_2. 10μm cryosections were stained using a Dako rat anti-Ki-67 antibody (TEC-3; 74μg/mL) with Hoescht 33342 nuclear counterstain.

In vitro osteogenic lineage commitment studies Void-forming hydrogels were incubated over polystyrene substrates as per deployment studies, and were moved every 7 days to a fresh polystyrene plate. Osteogenic supplements (50μg/mL *L*-ascorbic acid and 10mM β-glycerol phosphate) were added to the media (DMEM with 10% FBS), which was changed every other day throughout the culture period. To mimic the conditions which would be used for osteogenic transplantation assays, the cell density in these studies was $2x10^7$ cells per mL of bulk gel (e.g. 10^7 cells/mL of composite void-forming hydrogel as 50% of the total gel volume is porogen not containing cells). After hydrogels had been removed from a substrate (e.g. at day 14), plates were washed extensively with PBS to remove non-adherent cells and retain only deployed cells that had adhered to the substrate. Cells were then lysed into a passive lysis buffer (Promega) to retain the enzymatic activity of alkaline phosphatase (ALP). The nuclear fraction was separated

from the ALP-containing cytosolic fraction by centrifugation at 14,000g for 20 minutes. DNA was liberated from the nuclear pellet using CyQuant lysis buffer (Invitrogen), and probed with Hoescht 33342. The content of DNA was estimated using a standard curve provided by Calf Thymus DNA (Invitrogen).

ALP activity of cytosolic fraction of samples was analyzed using the fluorescent ALP substrate, 4-MUP (Sigma). Briefly, cytosolic fractions of lysed cells or serially diluted calf intestine ALP standards were added to a black-bottomed 96-well plates, and combined with 4-MUP. Samples were incubated at 37°C for one hr, and then the fluorescence intensity of cleaved 4-MUP was measured using a Biotek Plate reader. The activity of ALP in each sample was then estimated using the standard curve. ALP activity at day 14 (representing the differentiation of cells deployed between one and two weeks following encapsulation) was normalized to DNA content. Only samples containing a threshold level of DNA (25ng) were used for this analysis.

In parallel with these studies, void-forming hydrogels containing D1 mMSC were fixed at day 14. Osteogenic lineage commitment of cells was further verified with immunofluorescence analysis of Collagen I expression, and Von Kossa staining. For both sets of analyses, void-forming hydrogels were fixed (4% paraformaldehyde to crosslink cells, followed by 100mM barium chloride to crosslink hydrogels), washed extensively in PBS, embedded into OCT and flash frozen in liquid N_2. 10µm cryosections were stained using anti-Collagen I antibody (ab34710, Abcam) with Hoescht 33342 nuclear counterstain. For Von Kossa staining, sections (25µm) were incubated in a 1% solution of silver nitrate (Sigma) under ultraviolet light for 20 minutes. Next, sections were rinsed in deionized water, and incubated in 5% sodium thiosulfate (Sigma) for 5 minutes before imaging (Olympus D70). For quantification of Collagen I staining, the mean fluorescence intensity was measured in 16 randomly selected regions of interest. Cellular regions within the gel were selected, so that intensity measurements would reflect the intensity of Collagen I expression in cells, rather than be confounded by porosity.

In vitro deployment studies

D1 mMSC were encapsulated either into the bulk phase of multi-component hydrogels in which the bulk component was comprised of 10 or 20mg/mL RGD-modified (0-10 RGD / polymer chain) MVG. The concentration of MSC was maintained at 2 million cells per mL of bulk gel. In studies on the effects of bulk hydrogel elastic modulus on MSC fate, 10mg/mL RGD-modified MVG was mixed with unmodified MVG and low M_w MVG to a final concentration of 20-50mg/mL MVG[2]. Bulk gel formulations are described in Table S2. Porogen fabrication parameters were varied. Hydrogels were cultured in phenol red free DMEM with 10% FBS and 1% penicillin/streptomycin, atop tissue culture polystyrene substrates. Every 3-7 days, matrices were moved aespetically to fresh wells. MSC viability within multi-component materials at various time-points, along with the overall number and morphology of cells, was assessed with Live/Dead Staining. The number of deployed cells at a given time-point was obtained by measuring the metabolic activity of the plate from which the gel was moved using the Alamar Blue Assay (Invitrogen), based on a standard curve obtained from serially-diluted D1 cells. This approach was validated against direct counts of cells (fig. S3) obtained over the first seven days of cell deployment.

DOI: 10.1038/NMAT4407

In vivo deployment studies Retrovirus was first produced using standard protocols in HEK293T packaging cells. 293T cells were transfected using TransIT 293 (Mirus, Madison, WI) according to the manufacturer's instructions with the pOC-mCherry retroviral vector together with expression vectors encoding the packaging proteins. Viral supernatants were collected starting 48 h after transfection, for four consecutive times every 12 h, pooled, and filtered through a 0.45 μm filter. Viral supernatants were then concentrated 100-fold by ultracentrifugation in a Beckman centrifuge, for 1.5 hr at 16500 rpm. D1 mMSC were transduced with the mCherry retrovirus by incubating these cells with viral stocks in the presence of 5 μg/ml polybrene (Sigma) and 90-100% infection was achieved 3 days later[13].

mCherry-D1 cells were then encapsulated into the bulk phase of pore-forming hydrogels, and composite gels were injected (2 x 10^6 cells per 100μL injection) into the subcutaneous space of Nu/J mice (Jackson) via 18-gauge needles. The overall level of mCherry fluorescence, proportional to cell density, was measured using a Caliper Life Sciences IVIS Xenogen imaging system. All animal experiments were performed according to established animal protocols.

Bone Regeneration Studies

Cranial Defect Studies Critically-sized (8mm) defects were made into the crania of 5 week old nude rats (Charles River). After drilling defects into rat skulls, the periosteoum was completely removed. After the defects were stabilized, human mesenchymal stem cells were delivered either by direct injection (saline bolus), via injection within a standard hydrogel, or via injection within a void-forming hydrogel. The total injection volume was 100μL. 12 weeks after cell implantation, rats were euthanized by CO_2 inhalation, and skulls were obtained. Rat skulls were encoded so that micro-computed tomography and histology could be performed in a blinded fashion.

Micro-computed Tomography analysis Rat skulls were wrapped in a moistened cotton mesh and placed in a custom-built radiolucent batch scanning acrylic tube. The scans were performed on a Viva40 micro-CT (Scanco Medical AG®), at a voltage of 55 kV and current of 145 μA, integration time of 314 ms. Voxel size was selected to be isotropic and fixed at 35.5 μm. The scan axis was adjusted to be normal to the subject frontal plane.

For characterization of 3D newly formed mineralized tissue in the cranial defects, a cylindrical region of interest (ROI) of 8 mm diameter x 2 mm height was placed in the defect area to include the original volume of the defect area. The resulting greyscale images from the ROI were segmented using a low pass Gaussian filter. A fixed global threshold of 545 mg HA/cm3 was selected as the best choice that allowed the rendering of mineralized tissue for all the in vivo groups. The threshold for callus mineralization was approximately 45 % attenuation of intact bone[14]. The standard for comparison was set by visually evaluating 10 random single tomographic slices from four samples per group to isolate the mineralised tissue and preserve its morphology while excluding unmineralised tissues.

Using the processed images, the following morphometric measurements were analyzed: (i) bone volume, and (ii) average tissue mineral density. All analyses were

performed on the digitally extracted callus tissue using 3D distance techniques (Scanco® software, Scanco Medical AG®, Brüttisellen, Switzerland; supplemental ref. 15).

Histologic Analysis of Bone Regeneration Following µCT analysis, rat skulls were decalcified and paraffin embedded (Mass Histology). Histomorphological analysis was performed on 5 µm thick histology sections of the central part of the skull defect. The sections were stained with hematoxylin and eosin, and images were taken with a Olympus D70 camera on a Nikon Eclipse E800 microscope. The image processing software, ImageJ, was used to quantify the percentage of newly formed bone. The calibrated scale bar from the microscope was used to set the scale on the ImageJ software.

All image acquisition and analyses were performed in a blinded manner. For a quantitative analysis of new bone formation, the following approach was used: initially, the original defect area was determined based upon the fact that the drill used to make the bone defect had an external diameter of 8mm. A line of 8mm length was drawn across the bone area to establish the original defect margins. Based upon these boundaries and the width of the skull at the defect margin, the original defect area was delineated using the drawing tool on Image J. The software calculated the surface area of the original bone defect. Secondly, isolated centers of new bone in the remaining defect area (not touching the margins of the defect) were delineated and the surface area calculated. Finally, the fraction of the defect occupied by bone forming centers was calculated by dividing the surface area of the isolated centers of new bone by the surface area of the original defect. Standard protocols were followed for Safranin O and Mason's Trichrome staining.

In situ Hybridization Analysis of Human Cells Remaining at the Transplant Site after One Month Oligonucleotide probes against the primate specific *Alu* repeat sequence were purchased from Biogenix (Fremont, CA). Four weeks following transplantation of human MSC into nude rat cranial defects, rats were euthanized and skulls were decalcified. The decalcified histological sections (5µm) from the central defect region underwent deparaffinization and heat induced target retrieval in citrate buffer, pH 6.00 (RNase free) for 20 minutes. After post-fixation in 1% formaldehyde under RNase free conditions, the sections were then probed for the *Alu* repeat sequence (fluorescein-labeled oligonucleotide probe) using the protocol provided by the manufacturer and covered with a siliconized coverslip. Slides were heated for 5 minutes at 85°C and incubated in a moist chamber overnight at 37°C. Post-hybridization washes were followed by an in situ hybridization detection system utilizing a mouse anti-fluorescein antibody (BioGenex) and goat anti-mouse Alexa 568 (Invitrogen) labeled antibody and DAPI (Vector Laboratories) nuclear counterstain. The sections were evaluated with a fluorescent microscope (Nikon) and imaged (Olympus D70 camera).

DOI: 10.1038/NMAT4407

Table S.1 Polymer Formulations used to form porogens

Alginate Type	Degradable Component backbone modification	Non-degrading component backbone modification	Weight % Degradable Polymer	Weight % Non-Degradable Polymer
MVG	3-7.5% theoretical degree of oxidation[16]	None	2	0-1

Table S.2 Polymer formulations used to form bulk phase of hydrogels

Bulk gel modulus	Modification of cell-adhesive component	Non-degrading component backbone modification	Weight % RGD-modified high M_w MVG	Weight % Non-adhesive high M_w MVG	Weight % 5 Mrad MVG
5 or 20 kPa	10 RGD peptides / polymer chain	None	1	0	0
60 kPa	0-10 RGD peptides / polymer chain	None	1-2	0-1	0
110 kPa	10 RGD peptides / polymer chain	None	1	1	3

Figure S1

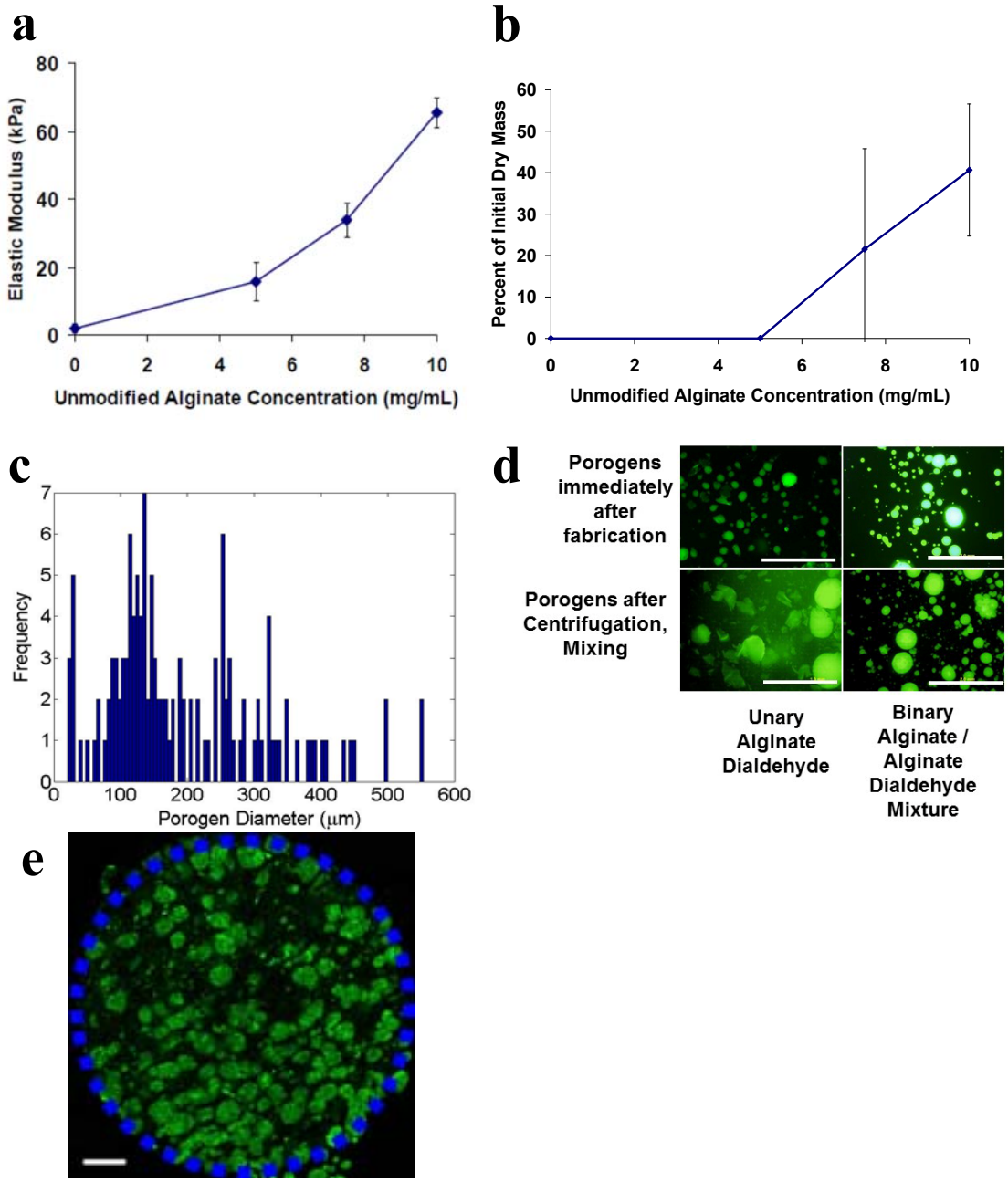

Mechanical properties and *in-vitro* degradation of porogen-forming hydrogel materials made using binary alginates. (a-b). Elastic moduli (a) and degradation (b) of bulk hydrogels formed by crosslinking binary combinations of oxidized alginate (5% theoretical degree of oxidation) at a constant density of 20mg/mL with unmodified, high M_w alginate. Degradation was assessed by comparing the dry mass after 4 days *in-vitro* to initial dry mass. **(c).** Histogram of diameters of porogens formed from binary mixtures of 20mg/mL oxidized alginate with 7.5mg/mL unmodified alginate. Porogen diameter was measured by processing fluorescent micrographs of porogens prepared from

DOI: 10.1038/NMAT4407

aminofluorescein-labeled alginates. **(d).** Representative fluorescence micrographs of porogens prepared from binary mixtures of high M_w, GA rich alginate with hydrolytically degradable oxidized alginate, or only completely from oxidized alginate, either immediately after fabrication or after processing steps used to remove excess crosslinker. **(e).** Representative confocal micrograph of porogens formed from aminofluorescein-labeled alginates, after encapsulating into unlabeled bulk gels, for quantitative fluorescence assay of porogen degradation (fig. 1c,d) of main manuscript. For these studies, the porogens were comprised of a mixture of 7.5mg/mL unmodified alginate with 20mg/mL of alginate dialdehyde that had a 5% theoretical degree of oxidation and was labeled with an average of 2 aminofluorescein molecules per alginate dialdehyde chain. Error bars: *SD*, n = 3-4. Scale bars: d: 2mm; e: 1mm.

Figure S2

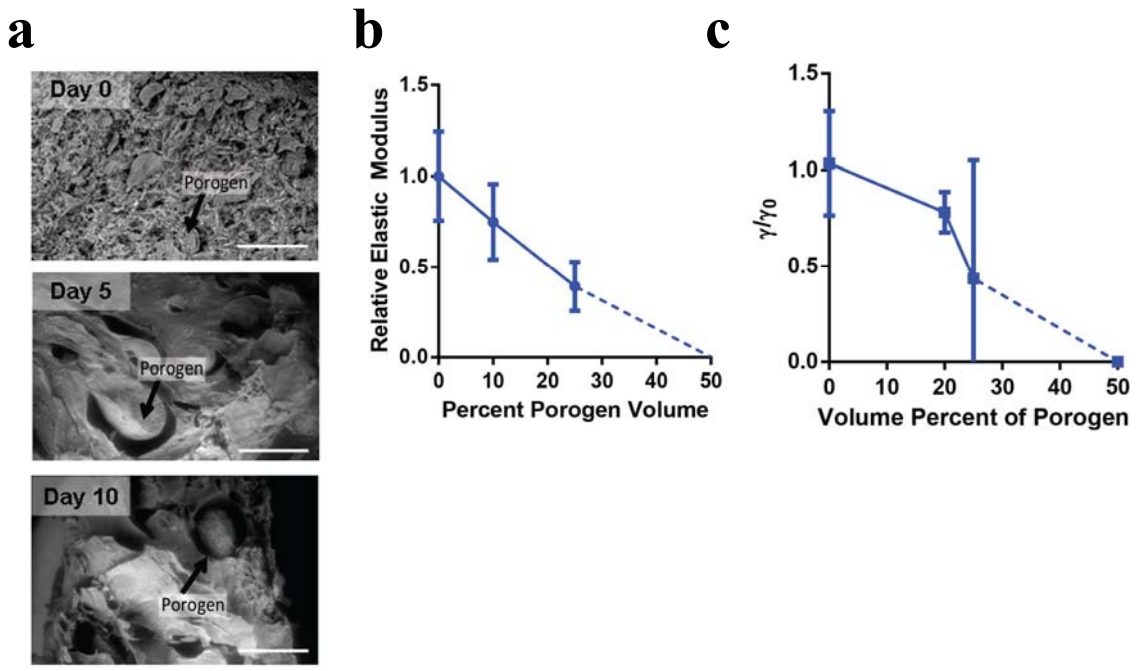

Additional Materials Characterization of Void Formation. (a). Scanning electron micrographs obtained by flash-freezing and sectioning void-forming hydrogels either 0, 5 or 10 days after gel formation and subsequent incubation in serum free media at 37°C. Porogens are denoted in images. **(b-c).** Analysis of the (b) relative elastic moduli and (c) relative fracture toughness of void-forming gels with varying volume percent of porogen, after forming composite gels and incubating in serum free media at 37°C for (b) 7 days or (c) 3 days. Regions indicated by dashed lines in denote that at 50% porogen density, the modulus and fracture toughness of these materials fell below the detection limit of the Instron mechanical testing apparatus. Error bars are *SD*, $n = 4$ (b) or $n = 2$ (c). Scale bars: a: 1mm.

DOI: 10.1038/NMAT4407

Figure S3

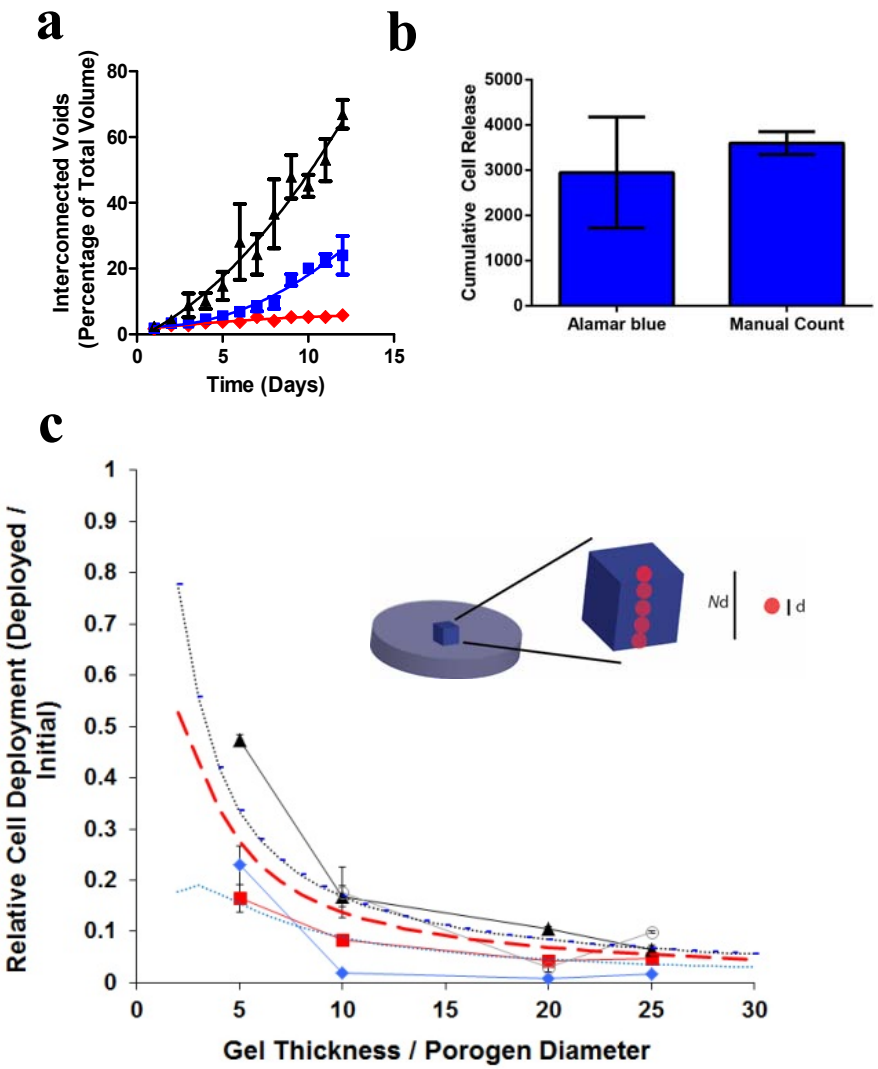

Analysis of interconnected void formation and cell release at sub-percolation porogen densities, and validation of alamar blue reduction assay for quantifying number of cells deployed from void-forming hydrogels *in-vitro*. (a). Kinetic analysis of percolating void formation by capillary assay of void forming hydrogels with 50% (◆), 65% (■) or 80% (▲) volume fraction of porogens. **(b).** Comparison of seven day cumulative release as measured by alamar blue analysis of metabolic activity of released cells, after they have adhered to plastic underneath gel discs, to cumulative cell release measured by directly trypsinizing cells off the substrate and counting with hemacytometer. Differences are not statistically significant ($p = 0.27$, two-way t-test). **(c).** Inset: schematic illustrating the arbitrary volume of void-forming hydrogels used to estimate the probability of cells being deployed from gels with a specified thickness of N porogens with diameter d. Graph: Analysis of relative mMSC deployment (cumulative number of cells deployed normalized to initial number of cells encapsulated) from void-

forming hydrogels as a function of gel size relative to porogen size for 25% (◆), 50% (■), 65% (▲), or 80% (●) porogen volume fraction. Dotted curves represent the numerical prediction of a cell being released from a void-forming hydrogel with a fixed initial porogen density (dotted black curve: 65%, dotted red curve: 50%, dotted blue curve: 25%) as the ratio of gel thickness to porogen diameter increases. Note, the relative actual number of cells released for void-forming hydrogels with sub-percolation density (< 65%) porogen densities were less than these numerical predictions, suggesting that the formation of interconnected networks of voids alone could account for cell release. Error bars: *SD*, n = 6-9.

DOI: 10.1038/NMAT4407

Figure S4

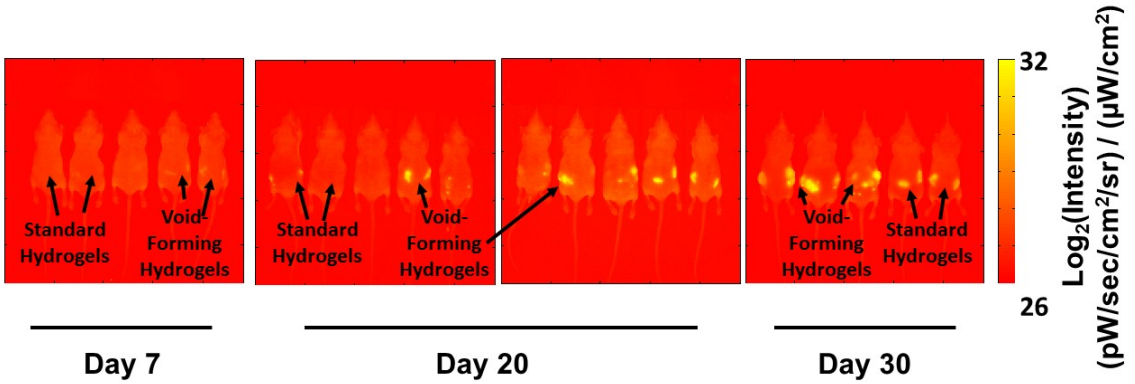

Representative images depicting detection limits of IVIS live animal imaging system. Representative images of Nu/J mice at day 7 (left), day 20 (center two images) and day 30 (right) after injecting D1-mCherry within void-forming gels or standard gels. To allow visual comparison between time points, data are plotted on a universal $\log_2$ scale. Note that each mouse received bilateral injections with gels, subcutaneously in above the hind limb. Note also, a lower-limit on quantitative detection of cells at day 7 (left), where background autofluorescence is at similar levels to mCherry fluorescence.

Figure S5

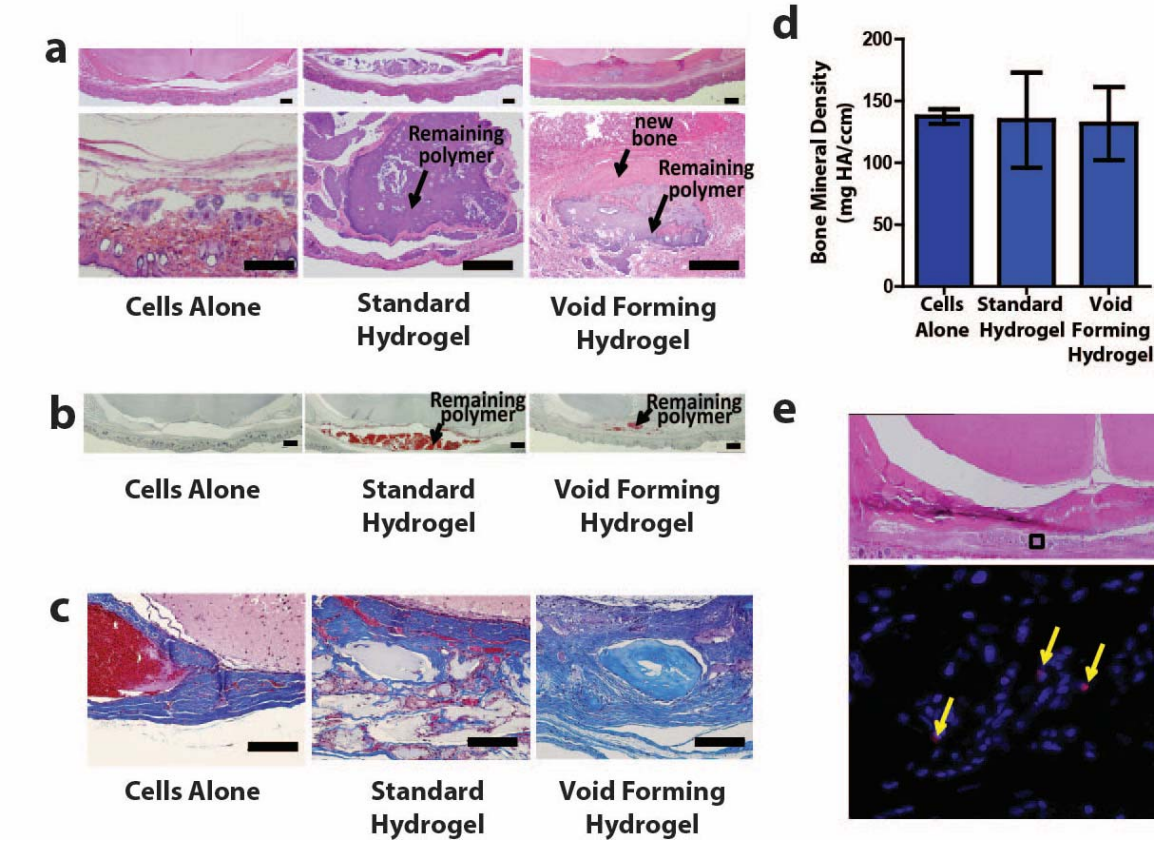

Analysis of the mineral density and histological features of new bone formation influenced by human MSC transplanted in standard and void-forming hydrogels with osteogenic mechanical properties. (a). Representative histology (Hematoxylin-Eosin staining) of new bone formation. **(b).** Representative Safranin-O staining (red) for residual alginate gel. **(c).** Representative Masson's Trichrome staining of new bone formation. **(d).** Mineral density of bone formed by human MSC transplanted into cranial defects. In all panels, data are shown for hMSC transplantation by saline bolus, within standard hydrogels, or within void-forming hydrogels. **(e).** Top: representative Hematoxylin-Eosin stain, with noted region containing the void-forming hydrogel, at one month after transplantation. To identify human MSC, the region shown was probed for the primate specific *Alu* repeat mRNA sequence. Bottom: representative fluorescence image from fluorescence in situ hybridization analysis showing primate specific *Alu* repeat mRNA sequence (red) with DAPI nuclear counterstain (blue). Scale bars: 100μm.

DOI: 10.1038/NMAT4407

Supplemental References

1. Bouhadir KH, Hausman DS, Mooney DJ. Synthesis of cross-linked poly(aldehyde guluronate) hydrogels. *Polymer* 1999; 40(12): 3575-84.

2. Huebsch N. *et al.* Harnessing Cellular Engineering of the Cell-Matrix Interface to Control Stem Cell Fate. *Nat Mater.* 2010; 9(6): 518-26.

3. Kong HJ, Chan JH, Huebsch N, Weitz D, Mooney DJ. Noninvasive probing of the spatial organization of polymer chains in hydrogels using fluorescence resonance energy transfer (FRET). *J Am. Chem. Soc.* 2007; 129(15): 4518-9.

4. Kong HJ, Lee KY, Mooney DJ. Decoupling the dependence of rheological/mechanical properties of hydrogels from solids concentration. *Polymer* 2002; 43: 6239-46**.**

5. Kong HJ, Smith MK, Mooney DJ. Designing alginate hydrogels to maintain viability of immobilized cells. *Biomaterials* 2003; 24: 4023-9.

6. Rowley JA, Madlambayan G, Mooney DJ. Alginate hydrogels as synthetic extracellular matrix materials. *Biomaterials* 1999; 20: 45-53.

7. Rivlin RS, Thomas AG. Rupture of rubber. 1. Characteristic energy for tearing. *J. Polym. Sci.* 1953; 10(3): 291-318.

8. Shapiro L, Cohen S. Novel alginate sponges for cell culture and transplantation. *Biomaterials* 1997; 18(8): 583-90.

9. Lorenz CD, Zigg RM. Precise determination of the critical percolation threshold for the three-dimensional "Swiss cheese" model using a growth algorithm. *J Chem. Phys* 2001; 114(8): 3659-61.

10. Care CM, Ettelaie R. Improved Rosenbluth Monte Carlo scheme for cluster counting and lattice animal enumeration. *Phys. Rev. E.* 2000; 62(1): 1397-404.

11. Pittenger MF, *et al.* Multilineage potential of adult human mesenchymal stem cells. *Science* 1999; 84: 143-7.

12. Diduch DR, Coe MR, Joyner C, Owen ME, Balian G. Two cell lines from bone marrow that differ in terms of collagen synthesis, osteogenic characteristics, and matrix mineralization. *J Bone Joint Surg Am* 1993; 75: 92-105.

13. Mammoto T, *et al.* Angiopoietin-1 requires p190 RhoGAP to protect against vascular leakage in vivo. *J Biol Chem.* 2007; 282(33): 23910-8.

14. Mehta M, Checa S, Lienau J, Hutmacher D, Duda GN. *In vivo* tracking of segmental bone defect healing reveals that callus patterning is related to early mechanical stimuli. *Eur J. Cell. Mater.* 2012; 24: 358-71.

15. Hildebrand T, Ruegsegger P. A new method for the model-independent assessment of thickness in three-dimensional images. *J Microsc*. 1997; 185: 67-75.

16. Bouhadir KH, Lee KY, Alsberg E, Damm KL, Anderson KW, Mooney DJ. Degradation of Partially Oxidized Alginate and Its Potential Application for Tissue Engineering. *Biotechnol. Prog.* 2001; 17: 945-50.